YITP-97-13

Particle production in quantum transport theories

P. Bożek *

Yukawa Institute for Theoretical Physics, Kyoto University, Kyoto 606-01 , Japan

and

Institute of Nuclear Physics, 31-342 Kraków, Poland

(February 4, 2008)

Abstract

The particle production in the intermediate energy heavy ion collisions is discussed in the framework of the nonequilibrium Green's functions formalism. The evolution equations of the Green's functions for fermions allows for the discussion of the off-shell fermion propagator and of the large momentum component in the initial state. For the case of a homogeneous system numerical calculations of the meson production rate are performed and compared with the semiclassical production rate.

24.10-i, 25.75Dw

*electronic mail : bozek@solaris.ifj.edu.pl

I. INTRODUCTION

The production of particles in the interacting nuclear medium has been a rich field of study [1]. The particle production is a quantity which can be to a large extent estimated in theoretical models. The particle production was used as a tool of the study of the highly nonequilibrium dynamics in the early stage of the nuclear collision and also as a probe of the behavior and a characteristic of the almost equilibrated system reached in the course of the collision. The estimation of the particle production probability usually is based on the free production cross section with some possible medium modifications included. This production cross section, taken for the 2-nucleon collision process, is used in the semiclassical Boltzmann-Uehling-Uhlenbeck (BUU) type simulations of the nuclear dynamics. A completely different approach to the particle production emerges from the quantum transport equations. The importance of the quantum transport description was realized in the correct treatment of the Landau-Pomeranchuk-Migdal effect in medium [2]. The approach based on the quantum transport equations takes into account the finite time extent between successive collisions and regularizes the divergent cross section for long-wavelength photons which require large formation time.

Two problems related to the particle production in intermediate energy heavy ion collisions are particularly interesting : the subthreshold meson production and the medium modifications of the meson properties. The production of the particles below the nucleon-nucleon energy threshold requires the presence of some additional mechanism in nuclear medium allowing for the production. Besides the obvious Fermi motion of nucleons, additional mechanisms could include the initial high momentum component in the nucleus and the many nucleon collisions. These phenomena can be treated in a unified way in the quantum nonequilibrium Green's function formalism [3–5]. The medium modification of the meson properties include the possible mass shift and width modifications in medium. If this occurs, a natural question arises also about possible strong medium modifications of the production rates. In the case of very strong medium modification of the meson properties

the meson production should be treated in a quantum transport framework.

In this work it will appear that the difference between the quantum and semiclassical production rates is very important. Usually one estimates the off-shell effects by taking a generalized parameterization of the fermion spectral functions in the calculation of the meson production rate in 2-nucleon collision. However, in the quantum transport equation the perturbative expansion using resumed fermion propagators is organized differently. The first nonzero contribution to the meson production comes from the one-loop diagram and its contribution is generally large. Another way of discussion of the subthreshold particle production is to estimate the particle production in 3 or more nucleon collisions processes. A large class of such meson production processes involving many nucleons is included in the one-loop meson self-energy with interacting off-shell fermion propagators.

In the present work in order to make a detailed estimation of the quantum and semiclassical production rates in the same system we will use a simple model. In this model of self-interacting nonrelativistic fermions weakly coupled to mesons we will calculate the one-loop quantum meson production rate and the corresponding semiclassical rate from the 2-nucleon collision process. Clearly we cannot use the free on shell meson production cross section as a starting point. Instead we will use a simple meson-nucleon coupling and we will derive the corresponding semiclassical production rate. The numerical calculations of the dynamics of the fermion Green's functions are done in a similar way as in the work of Danielewicz [6]. The production rate of mesons is estimated in a perturbative way, i.e. we assume that it is small and that the meson production does not modify the fermion dynamics.

In order to make the calculation feasible we assume that the system is spatially homogeneous. The quantum evolution equations are much simpler in this case, since the momentum integrals are the same as in the usual evaluation of perturbative diagrams and only the time integration must be done on a contour in the complex time plane. From the experimental evidence it seems as well established that the particle production around the threshold, but sufficiently above the absolute threshold, is an incoherent process. The number of produced

mesons scales very well with the number of participants. The result of the calculation in the homogeneous system giving the particle production rate per unit volume can be scaled to the size of the actual system under consideration. Thus, we believe that our results could be used for actual estimates of the production probability. Of course this would require the use of realistic meson nucleon vertices, and also the inclusion of the delta degrees of freedom. Our goal in this work is restricted to the presentation of the particle production in the nonequilibrium transport equations, with comparison to the semiclassical production rates. However, as a good motivation one should keep in mind the fact that the comparison of the particle production estimated in the off-shell Green's functions framework would represent a powerful test of the quantum effects. The particle production is one of the rare observables which can be reasonably well estimated in a homogeneous system and then compared to the experimental production rate per participant. Only the estimation of the absorption of the produced mesons must be done in a finite system. The difference in the transport coefficients between the quantum and the semiclassical evolutions discussed up to now [6–9] is not directly observable and could be effectively included in a medium modification of the nucleon-nucleon cross section.

II. PARTICLE PRODUCTION IN QUANTUM TRANSPORT EQUATIONS

We will consider a system of nonrelativistic interacting fermions. The first numerical solution of the Kadanoff-Baym equations for a homogeneous system was presented in Ref. [6]. For the dynamics of the fermions we follow the same approach. In sections II B and II C we will calculate the meson production rate in the system of interacting off-shell fermions.

A. Quantum transport equations for fermions

In this section we recall the notation of [3,4] and the numerical procedure for the solution of the nonequilibrium dynamics of fermion Green's functions. The Hamiltonian of fermions

interacting with a two-body potential V, can be written using the annihilation and creation operators $\hat{\psi}(x)$ and $\hat{\psi}^\dagger(x)$ as follows :

$$\hat{H} = \int dx\ \hat{\psi}^\dagger(x)\frac{-\nabla^2}{2m}\hat{\psi}(x) + \frac{1}{2}\int dx \int dy\ \hat{\psi}^\dagger(x)\hat{\psi}^\dagger(y)V(x-y)\hat{\psi}(y)\hat{\psi}(x)\ . \tag{1}$$

The spin and isospin indices are not written explicitly and we take a scalar potential for simplicity. The one-body evolution of the system can be described by the Green's functions :

$$\begin{aligned} G^<(x_1,t_1,x_2,t_2) &= i < \hat{\psi}^\dagger_H(x_2,t_2)\hat{\psi}_H(x_1,t_1) > \ , \\ G^>(x_1,t_1,x_2,t_2) &= -i < \hat{\psi}_H(x_1,t_1)\hat{\psi}^\dagger_H(x_2,t_2) > \ , \end{aligned} \tag{2}$$

where the field operators ψ_H are in the Heisenberg representation and the average $< \ldots >$ is the average over the initial state. These Green's functions are a particular case of the general contour time ordered Green's function :

$$G(x_1,t_1,x_2,t_2) = i < T_C\hat{\psi}^\dagger_H(x_2,t_2)\hat{\psi}_H(x_1,t_1) > \ , \tag{3}$$

where the field operators are ordered according to the time on the contour in the complex plain (Fig 1). For t_1, t_2 on different branches of the real time part of the contour the Green's function G can be replaced by two Green's functions $G^{<(>)}$ defined on the real line. In a spatial homogeneous system there is no dependence on the macroscopic coordinate $\frac{x_1+x_2}{2}$, and after Fourier transforming in the relative coordinate $x_1 - x_2$ we obtain the Green's function in momentum space $G^{<(>)}(p,t_1,t_2)$. The evolution of the system starting at some time t_0 can be described by the Schwinger-Dyson equations :

$$\begin{aligned} i\frac{\partial}{\partial t_1}G(p,t_1,t_2) - \omega_p G(p,t_1,t_2) &= \delta_C(t_1,t_2) + \int_C dt^{'}\Sigma(p,t_1,t^{'})G(p,t^{'},t_2) \\ -i\frac{\partial}{\partial t_2}G(p,t_1,t_2) - \omega_p G(p,t_1,t_2) &= \delta_C(t_1,t_2) + \int_C dt^{'}G(p,t_1,t^{'})\Sigma(p,t^{'},t_2)\ , \end{aligned} \tag{4}$$

where $\Sigma(p,t_1,t_2)$ is the self-energy which must be calculated in some approximation, $\delta_C(t_1,t_2)$ is the delta function on the contour and the time integration $t^{'}$ is done on the contour (Fig. 1). We neglect the mean field potential and the medium modification of the

nucleon effective mass, so that $\omega_p = \frac{p^2}{2m}$. For t_1, t_2 real and on different branches of the contour we obtain the Kadanoff-Baym equations :

$$
\begin{aligned}
i\frac{\partial}{\partial t_1}G^<(p,t_1,t_2) - \omega_p G^<(p,t_1,t_2) = & \left(\int_{t_0+i\tau_0}^{t_0} + \int_{t_0}^{t_1}\right) dt^{'}\Sigma^>(p,t_1,t^{'})G^<(p,t^{'},t_2) \\
& + \int_{t_1}^{t_2} dt^{'}\Sigma^<(p,t_1,t^{'})G^<(p,t^{'},t_2) \\
& + \left(\int_{t_0}^{t_0-i\tau_0} + \int_{t_2}^{t_0}\right) dt^{'}\Sigma^<(p,t_1,t^{'})G^>(p,t^{'},t_2) \ , \\
i\frac{\partial}{\partial t_1}G^>(p,t_1,t_2) - \omega_p G^>(p,t_1,t_2) = & \left(\int_{t_0+i\tau_0}^{t_0} + \int_{t_0}^{t_2}\right) dt^{'}\Sigma^>(p,t_1,t^{'})G^<(p,t^{'},t_2) \\
& + \int_{t_2}^{t_1} dt^{'}\Sigma^>(p,t_1,t^{'})G^>(p,t^{'},t_2) \\
& + \left(\int_{t_0}^{t_0-i\tau_0} + \int_{t_1}^{t_0}\right) dt^{'}\Sigma^<(p,t_1,t^{'})G^>(p,t^{'},t_2) \ , \qquad (5)
\end{aligned}
$$

and similar equations for the evolution in t_2. The description of the fermion evolution using only the one-body fermion Green's function involves the assumption that there are no 2 or many nucleon correlations present at the initial time [10,4]. Such many-nucleon correlations could be important for some processes involving nucleons in nuclei [11].

The actual solution requires first the solution on the imaginary time part of the contour, which is done iteratively. Then the Kadanoff-Baym equations are solved on the real time part of the contour. Also similar equations are solved for the case where one of the time arguments of the Green's function is on the real part and the other one is on the imaginary part of the contour. Of course the Hamiltonian of the evolution on the imaginary part of the contour must be modified. Otherwise we would always obtain the ground state of the one-body evolution with the Hamiltonian (1), for $\tau_0 \to \infty$. This can be done as an additional constraint or some modification of the Hamiltonian on the imaginary part of the contour. We will describe the nuclear collision as the equilibration of two counter-streaming flows of nuclear matter. Accordingly we choose, following [6], as the initial state two Fermi spheres of radius $p_f = 255 MeV/c$ centered at $\pm\frac{p_{coll}}{2}$ with the kinetic energy of the Hamiltonian on the imaginary part of the contour $\frac{p_T^2+(|p_L|-p_{coll}/2)^2}{2m}$ instead of $\frac{p^2}{2m}$ on the real part of the contour. The resulting evolution of the fermion Green's function is the so called evolution with correlated initial state. The self energy is taken in the direct Born approximation :

$$\Sigma^{<(>)}(p,t_1,t_2) = 4\int \frac{d^3p_1}{(2\pi^3)}\int \frac{d^3p_2}{(2\pi)^3} G^{>(<)}(p_1,t_2,t_1)$$
$$G^{<(>)}(p_2,t_2,t_1)G^{<(>)}(p+p_1-p_2,t_2,t_1)V(p_2-p)^2 \ , \qquad (6)$$

which allows for an efficient numerical evaluation. The factor 4 comes from spin isospin trace and the potential $V(p) = \pi^{3/2}\eta^3 V_0 exp(-\frac{p^2}{4\eta^2})$ ($V_0 = 453MeV$, $\eta = 0.57fm$) should be thought of as a local approximation to the T matrix.

Another possibility is to use only the real part of contour for the calculation of the evolution of the system. The fermion momentum distribution at $t = t_0$ is taken as two Fermi spheres. The kinetic energy in this case is increased in the course of the evolution and the final distribution corresponds the equilibrium distribution with higher temperature than in the case of the evolution including also the imaginary part of the contour. This real time only quantum transport evolution of the fermion system will be refered to as the evolution from an uncorrelated or a Hartree initial state.

We have used an axially symmetric system for the evolution of the Kadanoff-Baym equations, with momentum grid of $46MeV/c$ and of the size $|p| < 920MeV/c$. The imaginary time evolution was done for $\tau_0 = 3fm/c$ and the real time evolution was done for $20fm/c$. The momentum integrals are done by a Fourier-Bessel transformation and the time integrals are done in a usual numerical integration for each pair of times t_1, t_2 ($t_1 > t_2$).

B. Meson production

The meson production can be analyzed in a model where in addition to the Hamiltonian $\hat{H}$ for interacting fermions (1) we have a meson-fermion interaction vertex and of course the meson kinetic energy term. For the meson-fermion interaction we could take the form of the interaction as in the pion-nucleon case [13] :

$$\hat{H}_I = g\int dx \left(\hat{\psi(x)}^\dagger \sigma^i \partial_i \hat{\phi}_j(x)\tau^j \hat{\psi(x)} + \hat{\psi(x)}^\dagger \sigma^i \partial_i \hat{\phi}_j(x)^\dagger \tau^j \hat{\psi(x)}\right) \ , \qquad (7)$$

where $\hat{\phi}$ is the pion field operator, τ and σ are the isospin and spin matrices. The interaction strength g incorporates in general a momentum dependent form factor. However, in our

study the detailed structure of the interaction vertex is not important. Both in the one-loop diagram and in the semiclassical production rate the meson self-energy acquires the same coefficient from the meson-fermion interaction vertex. In the case of the interaction vertex written above (7), we have a common factor :

$$\lambda^2 = 4g^2q^2 \ , \tag{8}$$

in the momentum space, where q is the momentum of the meson. The interaction denoted in the following by λ^2 could be used also for any kind of meson-nucleon vertex, after taking the spin isospin trace. In the present study, which is a first estimation of the quantum production rate, we will not be interested in the detailed predictions. Instead we will calculate the rates of the meson production scaled by $1/\lambda^2$ for the comparison of the quantum transport equations and the semiclassical equations. Also we will treat the meson mass as a free parameter, performing the calculation for several different masses of produced particles.

The evolution of the nucleon meson system can be analyzed in the same way as the system of fermions, discussed in the previous section. The meson Green's functions can be defined as :

$$\begin{aligned} D^<(x_1,t_1,x_2,t_2) &= -i < \hat{\phi}^\dagger_H(x_2,t_2)\hat{\phi}_H(x_1,t_1) > \ , \\ D^>(x_1,t_1,x_2,t_2) &= -i < \hat{\phi}_H(x_1,t_1)\hat{\phi}^\dagger_H(x_2,t_2) > \ , \end{aligned} \tag{9}$$

where in the following we restrict our study to one meson species. The meson nucleon interaction induces a backreaction of the produced mesons on the fermion evolution. However we will suppose that the meson-nucleon vertex is weak, and that the meson production does not modify the fermion dynamics. The fermions do interact by the interaction V which induces the equilibration of fermions and leads to nonzero width of the fermion Green's functions. Thus, the meson production can be calculated from the known fermion Green's functions. We can write also the Kadanoff-Baym evolution equations for mesons :

$$\begin{aligned} i\frac{\partial}{\partial t_1}D(p,t_1,t_2) - \Omega_p D(p,t_1,t_2) &= \delta_C(t_1,t_2) + \int_C dt^{'}\Pi(p,t_1,t^{'})D(p,t^{'},t_2) \\ -i\frac{\partial}{\partial t_2}D(p,t_1,t_2) - \Omega_p D(p,t_1,t_2) &= \delta_C(t_1,t_2) + \int_C dt^{'}D(p,t_1,t^{'})\Pi(p,t^{'},t_2) \ , \end{aligned} \tag{10}$$

where Π is the meson self-energy and $\Omega_p = \sqrt{m_s^2 + p^2}$ is the relativistic meson kinetic energy. We take at this point the meson kinetic energy in the relativistic form in order to have a correct estimate of the energy of the meson for any meson mass and momentum. Otherwise the mesons are treated in an analogous way as the nonrelativistic fermions. The meson self-energy is taken in the one-loop form (Fig. 2). The equations (10) can be used for a complete study of the meson evolution in the nonequilibrium nuclear matter, including the in medium modifications of the meson properties, the meson production and absorption. In the present work we are interested only in the calculation of the meson production rate. It is equal to the rate of the change of the equal time meson Green's function $iD^<(p,t,t) = dN(p,t)/d^3p$, which is the meson momentum distribution in a homogeneous system . Supposing that the number of produced mesons is small, which is true for sufficiently small λ^2, we can neglect the meson occupancy on the right hand side of the equations (10), taking :

$$\begin{aligned} D_0^<(p,t_1,t_2) &= 0 \\ D_0^>(p,t_1,t_2) &= -i\exp\left(-i\Omega_p(t_1-t_2)\right) \ . \end{aligned} \tag{11}$$

This approximation is consistent with the neglect of the meson influence on the fermion dynamics. The production rate for mesons takes the form

$$\begin{aligned} \frac{dN(p,t)}{d^3pdt} = 2\mathcal{R}e\Bigg(&- \int_{t_0}^{t} dt^{'}\Pi^<(p,t,t^{'})D_0^>(p,t^{'},t) \\ &+ \int_{t_0}^{t_0-i\tau_0} dt^{'}\Pi^<(p,t,t^{'})D_0^>(p,t^{'},t)\Bigg) \ . \end{aligned} \tag{12}$$

The meson one-loop self energy is :

$$\Pi^<(p,t_1,t_2) = -i\lambda^2 \int \frac{d^3q}{(2\pi)^3} G^<(p-q,t_1,t_2)G^>(q,t_2,t_1) \ . \tag{13}$$

At this point, some comment is again welcomed concerning the integration on the imaginary part of the contour in the Kadanoff-Baym equations. We assume that the imaginary part of the evolution does not create mesons. This means again that we modify the Hamiltonian on the imaginary part of the evolution on the time contour, or equivalently that the evolution operator on the imaginary part of the contour includes a projection on the states

without mesons [14]. In this way we have no mesons at the initial time t_0. The problem of the presence of mesons in the initial state is by its own very interesting and could be addressed by the Kadanoff-Baym equations (4) and (10). The calculation of the meson distribution in the initial state would require a self-consistent solution of the interacting meson-fermion system. This is beyond the scope of the present work, where we restrict ourselves to the perturbative calculation of the meson production rate from the fermion Green's functions.

The rate of the meson production (12) consists of two time integrals, a real time and an imaginary time integration. For $t \to \infty$ the imaginary time integration is negligible, and we obtain as the production rate the imaginary part of the meson self-energy taken at the energy Ω_q. For finite integration times, the situation is different. In particular, taking the stationary fermion Green's functions on-shell :

$$\begin{aligned} G^<(p,t_1,t_2) &= if(p)\exp\left(-i\omega_p(t_1-t_2)\right) \ , \\ G^>(p,t_1,t_2) &= -i(1-f(p))\exp\left(-i\omega_p(t_1-t_2)\right) \ , \end{aligned} \tag{14}$$

we obtain from the real part of the time integration in Eq. (12) an oscillatory behavior :

$$\frac{dN(q,t)}{d^3qdt} = 2\lambda^2 \int \frac{d^3p}{(2\pi)^3} f(q-p)(1-f(p)) \ \frac{\sin\left((\Omega_q - \omega_{q-p} + \omega_p)t\right)}{\Omega_q - \omega_{q-p} + \omega_p} \ , \tag{15}$$

which only on average gives a zero production rate. On the other hand, taking the same form of the on-shell fermion Green's functions (14) also on the imaginary interval of the time integration in Eq. (12) and taking $\tau_0 \to \infty$ one obtains :

$$\frac{dN(q,t)}{d^3qdt} = 0 \ , \tag{16}$$

exactly for each t. Thus, we believe that the imaginary part of the time integration is important in the calculation of the production rate in a finite time interval after t_0. Of course in the system that we solve numerically we have off-shell Green's function which gives a nonzero production rate. Also in the far from equilibrium system at the beginning of the collision the Green's function depend strongly on the macroscopic time $\frac{t_1+t_2}{2}$. One should remember that even in the stationary case the analytical continuation of the self-energy from the imaginary to the real times is nontrivial and in fact it is possible only in

the perturbative calculation, when the analytical expressions for the self energy are known. The method presented above is way of calculating the real time quantities from the Green's functions evolved in the imaginary time. It would be interesting to analyze in details this problem in the case of a finite temperature stationary solution, i.e. in the case where the imaginary evolution is the usual finite temperature evolution over an imaginary time interval $1/T$ with the same Hamiltonian on the real and the imaginary part of the contour.

C. Numerical results for the quantum production rate

The numerical calculation of the fermion evolution was performed for the energy of the collision of $180MeV$ and $110MeV$/nucleon in the c.m.. We have calculated two evolutions of the fermion Green's functions, corresponding to a correlated or uncorrelated initial state. The evolution was followed up to $20fm/c$. At that time the fermion distribution is almost spherical and equilibrated. Also, at $t = 20fm/c$ there is already no influence of the initial part of the time contour on the evolution. However, the evolution for the initial correlated and the evolution for the initial Hartree state have different temperatures at large times. The temperature in the second case is larger and so is the meson production at large times. The calculation of the one-loop meson self energy is done in a similar way as for the fermion self-energy, i.e. by a Fourier-Bessel transform calculation of the convolution momentum integral in Eq. (13). For zero meson momentum the integration is done directly.

We have calculated the meson production in three ways. The first possibility is to take the Hartree initial state and the whole evolution of the fermion Green's functions is in the real times. For this case we calculate the meson production using Eq. (12) with only real time integration on the right hand side. For the case of the correlated initial state the evolution of the fermion Green's functions is performed both on the real and imaginary part of the contour in Fig. 1. The corresponding meson production rate can be calculated in two ways. One way is to integrate only over real times on the right hand side of Eq. (12), the other one is to take the whole expression (12). Of course, at large times, the two approaches give the

same result, since the contribution of the imaginary time integration is negligible for large times. However, at the beginning of the evolution, the differences are important. In most of the cases, the full expression (12) is well behaving, with less oscillatory behavior. The oscillatory behavior at the beginning of the evolution is due to the finite time integration. This gives only on average an expression for the production rate.

In Figs. 3, 4 and 5 is shown the time dependence of the scaled production rate $\frac{1}{\lambda^2}\frac{dN}{d^3qdt}$ for three different masses of the mesons 20, 140 and $300MeV$ respectively. We prefer to use the scaled production rate, since it allows us a general discussion. In particular, we can analyze the behavior around $q = 0$ where the production rate would be 0 if multiplied by the pion vertex strength. The general behavior is as expected, starting with oscillations until the asymptotic production rate settles in. This initial time dependence of the production rate is not due to the nonequilibrium character of the evolving system. Rather, it is due to the finite time integration in the expression for the production rate, as discussed above. For not very large values of the meson mass m_s or meson momentum q, i.e. not very far from the mass shell, we can parameterize the fermion Green's functions using a Lorentzian spectral function. In that case one expects that the oscillations in the production rate would be damped with a time $1/\Gamma$, where Γ is the average width of the spectral function. In our case the width is around $50MeV$ which should give a decay time of $4fm/c$ in accordance with the Figs. 3, 4 and 5. The asymptotic value of the production rate at large time is not zero. However, for large mass of the meson or large momentum of the meson the asymptotic value of the production rate is much smaller then the amplitude of the oscillations at the initial time. In order to get stable results for the case of large mass and/or momentum of the produced meson we had to use very small time step ($.067fm/c$ and $.15fm/c$ for the real and imaginary evolution respectively). This allows to get a correct estimate of the fermion spectral function far from the mass-shell. The asymptotic production rate of mesons is systematically larger for the evolution from the uncorrelated initial state (dashed lines in Figs. 3, 4 and 5). It is a manifestation of the the higher temperature reached in the equilibration of the uncorrelated initial state. In Fig. 6 is shown the time dependence of the

meson production rate for large times. For the case of meson of mass 140 and $300MeV$ an almost stationary production rate is reached. However for the mesons of mass $500MeV$ still oscillations of high amplitude are seen. These oscillations are slowly damped to a positive value corresponding to the asymptotic meson production rate.

In Fig. 7 is shown the production rate of mesons at large time ($t = 20fm/c$), as a function of the transverse momentum. At this time the production rate of mesons is almost isotropic. The quantum meson production rate for large meson energy was estimated as the average over its last oscillation in the time dependent meson production rate. Similarly as in the plots of the time development of the production rate, the production rate is larger for the uncorrelated initial state. One should note that the plots in Fig. 7 do not represent the genuine transverse momentum distribution of produced mesons, since the interaction strength λ^2 can in general depend quite strongly on the momentum of the produced meson q. In Fig. 8 is shown the total number of mesons produced during the evolution as a function of the transverse momentum. The highest number of mesons is produced in the evolution from an uncorrelated initial state. In the time integrated production rate, a big difference appears between the meson production calculated from the full expression (12) and the meson production calculated from the Eq. (12) including only the real interval of the time integration. The difference can be observed in the plots of the time dependence of the meson production rate for small times. The large oscillations of the production rate at small times give after time integration a large contribution. This contribution is unphysical, since in a nuclear collision there is no sudden switching on of the interaction at time $t = t_0$. The time integrations are always infinite and the production rate should not have the oscillations characteristic of the finite time integration. At each time the locally asymptotic, but not necessarily stationary, meson production rate can be defined, if the time integration would be much larger than the inverse fermion single particle width $1/\Gamma$. In the nonequilibrium Green's evolution presented in this work, we have to start from a finite initial time. The procedure with imaginary time integration in the initial state leads to a better description of the evolution of fermions and of the meson production rate.

Close to the mass-shell the fermion Green's functions are often parameterized as :

$$G^<(p,t_1,t_2) = if(p)\exp\left(-i\omega_p(t_1-t_2)-\Gamma_p|t_1-t_2|\right) \ ,$$
$$G^<(p,t_1,t_2) = -i(1-f(p))\exp\left(-i\omega_p(t_1-t_2)-\Gamma_p|t_1-t_2|\right) \ , \qquad (17)$$

and one gets for the meson production rate :

$$\frac{dN(q=0,t)}{d^3qdt} = \lambda^2\int\frac{d^3p}{(2\pi)^3}f(p)(1-f(p))\frac{4\Gamma_p}{m_s^2+\Gamma_p^2} \ . \qquad (18)$$

This formula gives Lorentzian dependence on the meson mass if the width Γ_p is weakly depending on momentum. In Fig 9 is shown the dependence of the asymptotic production rate of mesons at zero momentum as a function of the meson mass. This dependence is close to an exponential and cannot be approximated by a Lorentzian. In the appendix B is shown that even if the fermion spectral function is Lorentzian we do not get a Lorentzian dependence of the meson production rate on the meson mass, if we use a more general expression for the equilibrium Green's functions than the Eq. (17).

The fermion Green's functions obtained as a result of the numerical solution of the Kadanoff-Baym equations are very different from the parameterization (17) [6]. The function $f(p)$ in the above parameterization corresponds to the momentum distribution of fermions. However, we have found that the imaginary part of $-iG^{<(>)}(p,t_1,t_2)\exp(i\omega_p(t_1-t_2))$ is nonzero and gives an important contribution to the meson production rate. The Lorentzian parameterization of the spectral function is expected to be valid near the mass shell. Accordingly, it cannot be applied for the description of the meson production which involves the far from the mass-shell spectral function of fermions.

III. COMPARISON TO THE SEMICLASSICAL PRODUCTION RATE

The semiclassical meson production rate from a homogeneous BUU-like evolution of the collision will be presented. The BUU evolution is done for the Hartree initial momentum distribution and for the initial momentum distribution obtained from the imaginary time

evolution of the Kadanoff-Baym equations. Such calculations correspond to the standard approach to the meson production in nuclear collisions.

Other results will also be presented for the semiclassical production rate with fermion momentum distribution taken from the equal time Green's functions generated in the quantum evolution. It is interesting to compare the semiclassical meson production rate in a quasistationary state to the quantum production rate in the same system.

The semiclassical production rate is defined in App. A. In this chapter we use the expression (A1) and (A2), with $\gamma = 50MeV$.

A. Semiclassical evolution equations and meson production

The semiclassical evolution equation for fermion densities can be obtained from the Kadanoff-Baym equations [3–5]. We take the nucleon-nucleon scattering cross section corresponding to the direct Born fermion self energy :

$$\begin{aligned}\frac{df(p_1,t)}{dt} = &-\int \frac{d^3p_2}{(2\pi)^3}\int \frac{d^3p_3}{(2\pi)^3}\int \frac{d^3p_4}{(2\pi)^3} V^2(p_1-p_3) \\ &(2\pi)^3\delta^3(p_1+p_2-p_3-p_4)2\pi\delta(\omega_{p_1}+\omega_{p_2}-\omega_{p_3}-\omega_{p_4}) \\ &\Big(f(p_1,t)f(p_2,t)\left(1-f(p_3,t)\right)\left(1-f(p_4,t)\right) \\ &-f(p_3,t)f(p_4,t)\left(1-f(p_1,t)\right)\left(1-f(p_2,t)\right)\Big) \,. \end{aligned} \tag{19}$$

The initial momentum distribution of fermions $f(p,t_0)$, should be taken as two Fermi spheres separated in momentum space by the momentum of the collision. However, we know that the nuclei in the ground state are not Hartree states with with zero temperature. In particular they have a large momentum component in the fermion momentum distribution. In our model involving spatially homogeneous system, it can be described by taking as the initial state the Hartree state evolved on the imaginary time contour by the Kadanoff-Baym equations. This corresponds to allowing for the initial quantum correlations, which modify the momentum distribution. This effect is expected to be important for the subthreshold meson production rate. Accordingly, we will use also the fermion momentum distribution in

the correlated state as the initial momentum distribution $f(p, t_0)$. The average kinetic energy in the correlated state is around $10MeV$/nucleon larger than in the Hartree state. The momentum distribution in the correlated initial state has a large momentum component.

The BUU-like evolution following the semiclassical fermion collision term (19) was solved on the same momentum grid as the quantum evolution. The time step was taken equal to $0.5fm/c$. In the effectively 5 dimensional integration on the right hand of Eq. (19) 3 dimensions were integrated by Monte-Carlo integration and two momentum integration were summed over the momentum grid.

From the semiclassical fermion momentum distribution obtained from Eq. (19), we can calculate the semiclassical meson production rate using Eq. (A1). Another possibility is to use the fermion momentum distributions obtained from the quantum evolution equations :

$$f(p,t) = -iG^<(p,t,t) \ . \tag{20}$$

As the system in the quantum evolution reaches an almost stationary state after $20fm/c$ of real time evolution, we can compare the meson production rate in this stationary state as obtained from the quantum and the semiclassical expressions for the meson production. The two stationary states that we discuss below have different temperatures and correspond to the initial correlated state and the initial Hartree state in the quantum evolution equations.

B. Discussion of the results for the semiclassical meson production rate

The time dependence of the semiclassical production rate is very similar for different meson masses or momenta. Thus, we present only one Figure of the time dependence of the semiclassical production rate. In Fig. 10 is shown the time dependence of the semiclassical meson production rate for the meson momentum $q = 184MeV/c$ and for three different meson masses. At the initial time the semiclassical production rate has two values, depending on the initial state of the evolution. For the correlated initial state (dotted and dashed-dotted lines in Fig. 10) the production rate at the beginning of the evolution is

higher than for the Hartree initial state (solid and dashed lines in Fig. 10). It is due to the fact that the average kinetic energy in the correlated initial state is higher than in the Hartree state.

The BUU-like evolution from the initial Hartree state, has the lowest average kinetic energy. For the higher energies of the produced mesons, especially for the case of $\Omega_q = 352MeV$ (the lower panel), the semiclassical production rate increases during the evolution. Such a behavior is expected, since the system approaches thermal equilibrium with some small thermal high momentum tail. However, as the average kinetic energy is conserved, the final equilibrium state has the lowest semiclassical meson production rate among all the results presented in Fig. 10.

On the other hand, the quantum transport evolution starting from the initial Hartree state, leads to an increase of the kinetic energy. The initial correlation energy is changed into the kinetic energy [6,8]. As a result the average kinetic energy is increased by $30MeV/$nucleon and it is the largest among all the different evolutions considered in Fig. 10. Thus, it is obvious that also the semiclassical production rate would be the largest in this case. Within the first few fm/c the semiclassical production rate increases very fast. After this initial increase the meson production rate increases only slowly. This slow change of the semiclassical meson production rate is determined by the equilibration of the momentum distribution of fermions in the later stage of the Kadanoff-Baym equations evolution of fermions.

The two evolutions starting from the correlated initial state have very similar average kinetic energies during the whole evolution. Thus, the semiclassical meson production rate for the BUU-like evolution and for the quantum evolution from a correlated initial state are not very different (the dotted and dashed-dotted lines in Fig. 10). The BUU-like evolution starting from the correlated initial state can be considered as a model of the BUU evolution of the initial nucleon momentum distributions in nuclei that includes the large momentum tail of quantum origin (dotted line in Fig. 10). This kind of calculation represents all the quantum effects that can be taken into account in the approach using the 2-nucleon

process only and on-shell particles. To go beyond the discussion of the quantum effects in the initial state only, i.e. to include the off-shellness of the fermion Green's functions, requires an off-shell calculation of the meson production rate as was presented in Sect. II B and II C. The difference between the BUU evolution from the Hartree initial state and the BUU evolution from the correlated initial state is especially important for the case of the production of meson of mass $300MeV$. This meson mass corresponds to the subthreshold meson production, since the energy of the produced meson is $352MeV$ and the average c.m. energy is $180MeV$ (the kinematical limit for the meson production in the Hartree initial state is around $450MeV$). The ratio of the semiclassical meson production in the correlated initial state evolution and in the Hartree initial state evolution changes from 26 at $t = 0$ to 3 at $t = 20fm/c$. From Fig. 10 we see that the BUU-like evolution gives similar results as the the quantum evolution if the correlated initial state is used. The use of the initial correlated state is justified in the Kadanoff-Baym equations. It is a much more realistic way of starting the quantum transport equations evolution than the Hartree initial state.

We do not show in Fig. 10 the quantum meson production rate since the quantum rate is one order of magnitude larger. Moreover, the asymptotic quantum meson production rate can be defined only for large times. The large time quantum and semiclassical meson production rate as a function of the transverse momentum of the produced meson are compared in Fig. 11. The quantum meson production rate is about one order of magnitude larger than the semiclassical meson production rate. The dashed and the dotted line represent the quantum and semiclassical meson production rate for the larger temperature state reached in the evolution from the Hartree initial state. The solid and the dashed-dotted line represent the same for the evolution from the correlated initial state. From Fig. 11 we see that the semiclassical and the quantum meson production rates are very different for the same state reached in the evolution of the system. This is very different from Fig. 10, where we have seen that the differences between the semiclassical and quantum evolutions of the correlated initial state are not big if we are using only the semiclassical meson production rate formula.

In Fig. 12 we present the transverse momentum distribution of the meson production rate at $t = 20fm/c$ for the lower energy of the collision ($110MeV$/nucleon in the c.m.). The three "physically" well founded approaches are the quantum evolution from the correlated initial state, the BUU evolution from the correlated initial state [12] and the BUU evolution from the Hartree initial state (the solid, dashed-dotted and dotted lines in Fig. 12). Besides these results we plot the semiclassical meson production rate for the fermion momentum distribution calculated in the quantum evolution of the correlated initial state. Similarly as for the higher energy the semiclassical meson production rate is similar for the BUU and quantum evolved correlated initial state. Also similarly as in the results presented in Fig. 11 the quantum meson production rate is about one order of magnitude larger than the semiclassical meson production rate. The difference is even larger if compared to the semiclassical meson production rate for the BUU evolution of the Hartree state. We have used the same effective width $\gamma = 50MeV$ in the calculation of the matrix element for semiclassical meson production, as for the higher energy, since the single particle fermion width is reduced only by a few percent, when changing the initial energy. We do not show the results for $m_s = 300MeV$, because no asymptotic meson production rate could be estimated for this meson mass and large meson momentum.

IV. CONCLUSIONS

We have presented the first approach to the calculation of the meson production rate in the non-equilibrium quantum transport equations. The Kadanoff-Baym equations for the evolution of fermions were solved and the resulting off-shell fermion Green's functions were used for the calculation of the one-loop meson self-energy. The one-loop meson production rate shows strong oscillations at the beginning of the evolution of the system. This behavior comes from the fact that the time integral in the meson evolution equation is finite. Only after some time the meson production rate reaches some asymptotic value, which can be defined as the quantum meson production rate. We have found that the behavior of the

meson production rate at small times improves if the imaginary part of the time integration in the meson evolution equations is taken into account. We plan to study this question in details for the case where the fermion Green's functions on the imaginary and real parts of the time contour is the finite temperature Green's function corresponding to the same stationary finite temperature state.

The formalism based on the off-shell nucleon propagators allows to estimate the effects of the initial quantum correlations on the meson production rate. We have found that these initial correlations are important and that their inclusion increases the semiclassical meson production rate. This effect is especially important for the subthreshold meson production ($m_s = 300MeV$ in Fig. 10). The initial correlations in the fermion distribution can be evolved with BUU-like fermion evolution equation. Also the fermion momentum distribution can be obtained from the equal time fermion Green's functions calculated with the Kadanoff-Baym equations. Both calculations give similar average fermion kinetic energy and similar semiclassical meson production rate. Thus, it makes no dramatic difference in the semiclassical particle production if the nucleon momentum distribution is evolved according to the Kadanoff-Baym equations or according to the BUU equations, if the initial momentum distribution includes the quantum correlations.

The situation is very different if the quantum meson production rate is used to calculate the number of produced particles. In the system reached by the equilibration of the nuclear collision of the energy $180MeV$/nucleon in c.m, the quantum meson production rate is usually one order of magnitude larger then the semiclassical meson production rate. This is an important difference which requires detailed attention when discussing the particle production in a hot nuclear matter. The phenomenological consequences for the pion production may be less important since we discuss only the direct pion production process. The direct pion production is known to be less important than the delta production, at least in the semiclassical approach. The delta production should be less influenced by the nucleon off-shellness. However, as a result of our estimates the direct pion production should not be neglected in the total pion production yield if the quantum production rate

is used for the direct pion production. More detailed calculations using a model incorporating delta, nucleon and pion degrees of freedom is required to address quantitatively the phenomenological predictions for pion production. More work is also needed in the study of the parameterization of the retarded nucleon propagator which comes into the calculation of the semiclassical meson production rate. This could be studied first in the equilibrium state using the quantum transport equations.

In view of our results, the models of the particle production in the hot nuclear medium should be based on the Kadanoff-Baym equations, or should be based on off-shell transport equations [16]. Great care must be shown in the use of approximate fermion spectral functions. The numerical calculations show that the simple parameterizations of the fermion spectral function as in Eq. B1 does not give the correct quantitative result. This is even more pronounced for the less general parameterization of the fermion Green's function in Eq. (17), giving a qualitatively different dependence on the meson mass.

ACKNOWLEDGMENTS

The author would like to thank P. Danielewicz for useful discussion. Also, he gratefully acknowledges the hospitality extended to him by the YITP.

APPENDIX A: SEMICLASSICAL PRODUCTION RATES

The semiclassical production rate can be obtained from the cut diagrams, by putting the Greens functions $G^{<(>)}$ on shell [4,5,15]. This procedure leads to zero for the one-loop diagram (Fig. 2) that was discussed for the quantum production rate. The 3-body energy conserving delta function has no solution for our kinetic conditions. In the next order in V, only a vertex correction to the one-loop diagram appears. This also does not give any contribution on-shell. In the second order in the interaction V there appear 8 direct diagrams (Figs. 13, 14 and 15). There are 8 other exchange diagrams, that we will not discuss here since for the fermion evolution only direct diagrams are taken. The diagrams in Fig.

13 should not appear in the perturbative expansion, since they represent self-energy corrections on fermion lines. These are already included in the dynamically calculated fermion Green's functions. However, they should appear naturally in a perturbative expansion of the production rate in vacuum, using the on-shell Green's functions. The separation of the 3-body event which is the scattering with meson production from the succession of a 2-body scattering and successive meson emission can be done by the non-zero width in the retarded propagator in the diagrams in Figs. 13, 14 and 15 [15]. Of course the 2-body scattering and successive meson emission gives zero contribution on shell. If such a procedure is used, the diagrams in Fig. 13 are a first term in a series of diagrams involving the direct Born self-energy insertions on fermion lines. The sum of the diagrams in such a series should correspond to the one-loop meson-self energy diagram with resumed fermion Green's functions. One diagram of the next order in this series is shown in Fig. 16. The cutting procedure on the higher diagrams in this series leads to the processes involving many fermions on-shell. Such many nucleon processes should be taken into account in the calculation of the subthreshold particle production. The many nucleon processes, which can be obtained from the cutting of the direct Born self energy insertions, are resumed in the off-shell Green's functions calculated in Sect. II A. In the following we will take only the diagrams in Fig. 13 for the calculation of the semiclassical meson production rate. This correspond to taking only the 2-nucleon term in the expansion of the meson self energy in the number on interacting nucleons. The corresponding matrix elements is given below (A2) (Fig. 18). The diagrams in Fig. 15 are zero in the case of the interaction vertex (7) and also more generally for a large class of theories.

Identifying each cut propagator with the fermion Green's function on shell ($iG^{<(>)}$ depending on the direction of crossing the cut), and the propagator on the left (right) side of the cut with the retarded (advanced) propagator we obtain the following form of the meson production rate :

$$\frac{dN(q,t)}{d^3qdt} = \int \frac{d^3p_1}{(2\pi)^3}\int \frac{d^3p_2}{(2\pi)^3}\int \frac{d^3p_3}{(2\pi)^3}\int \frac{d^3p_4}{(2\pi)^3}|M|^2(2\pi)^3\delta^3(p_1+p_2-p_3-p_4-q)$$

$$2\pi\delta(\omega_{p_1}+\omega_{p_2}-\omega_{p_3}-\omega_{p_4}-\Omega_q)f(p_1,t)f(p_2,t)\,(1-f(p_3,t))\,(1-f(p_4,t))\ . \quad \text{(A1)}$$

Here analogously as for the calculation of the quantum production rate (sect. II B) we put the meson Green's function on shell and neglect the meson occupancy in the calculation of the production rate. The square of the matrix element $|M|^2$ in the above expression can be identified with the sum of the cut meson self-energy diagrams (Fig. 13, 14 and 15) with the cut fermion Green's functions $iG^{<(>)}$ factored out. The square of the matrix element $|M|^2$ can be written in the form of the diagram in Fig. 17 where the fermion Green's function is the retarded propagator and the external Green's functions have momenta corresponding to the integration momenta in Eq. (A1). The diagrams in Fig. 14 and 15 appear also in the expansion of the self-energy in the quantum transport equations, i.e. in the expansion using the resumed fermion propagators, but at a higher order in V. Thus in order to compare the semiclassical rate to the one-loop quantum rate, only the cut self-energy insertion diagrams (Fig. 13) should be taken. Clearly, even using the finite width for the retarded propagator in the semiclassical calculation no correspondence is found between the order of the perturbative expansion on shell and off shell. The cut diagrams in Fig. 14 and 15 give contributions of the same order as the cut self-energy insertion diagram (Fig. 13). However, in the quantum expansion theses diagrams are of different order. Moreover, already at the first order in V a vertex correction to the one-loop quantum diagram appears, which is still zero on-shell.

For the diagrams in Fig. 13 we obtain (Fig 18) :

$$|M|^2 = 4\lambda^2 V(p_2-p_4)^2\left(|\frac{1}{\omega_{p_1-q}+\omega_{p_2}-\omega_{p_3}-\omega_{p_4}+i\gamma}|^2 + |\frac{1}{\omega_{p_1}+\omega_{p_2}+\omega_{p_3+q}-\omega_{p_4}+i\gamma}|^2\right)\ . \quad \text{(A2)}$$

After the calculation of the traces over spin and isospin indices, the interaction g^2 and a factor $4q^2$ appear. This can be written in the same way as for the one-loop calculation, i.e. as λ^2. The additional factor 4 comes from the spin isospin trace in the second fermion loop. In most of the cases, unless otherwise stated, we use the production rate with constant

width parameter $\gamma = 50MeV$. This is the typical average fermion width as obtained from the quantum transport equations for fermions at the collision energies considered here. Of course in general it is momentum and time dependent, but in the calculation of the semiclassical production cross section we take a constant value of the fermion width.

APPENDIX B: MESON PRODUCTION IN EQUILIBRIUM

In this section we will present a simple estimate of the meson production in an equilibrium fermion system at finite temperature. For the fermion spectral function we will take the Lorentzian form. The fermion Green's functions, after Fourier transforming in the relative time variable, will be parameterized in the following way [3] :

$$G^<(p,\omega) = i\frac{\Gamma_p}{(\omega-\omega_p)^2+(\Gamma_p/2)^2} f_0(\omega) \ ,$$
$$G^>(p,\omega) = -i\frac{\Gamma_p}{(\omega-\omega_p)^2+(\Gamma_p/2)^2} (1-f_0(\omega)) \ , \tag{B1}$$

where we take a constant width Γ_p and

$$f_0(\omega) = \frac{1}{1+exp((\omega-\mu)/T)} \tag{B2}$$

is the equilibrium Fermi distribution at finite temperature ($T = 30MeV$, $\mu = 40MeV$, $\Gamma = 60MeV$, $|p| < 900MeV$, $|\omega - \omega_p| < 1800MeV$).

We have calculated the meson production from the one loop diagram :

$$\frac{dN(q=0)}{d^3q dt} = \lambda^2 \int \frac{d^3p}{(2\pi)^3} \int \frac{d\omega}{(2\pi)} G^<(p,\omega) G^>(p,\omega - M) \tag{B3}$$

The above equation is different from the Eq. (18) used in Sect. II C. Here we are using the general equilibrium form of the Green's functions [3] with a Lorentzian spectral function. As a result, the dependence of the meson production rate on the meson mass is almost exponential (see Fig. 19), similarly as in the numerical results in Fig. 9. This dependence is not Lorentzian as expected from Eq. (18). Even for Lorentzian spectral function with constant width the resulting dependence of the production rate on the meson mass is not

Lorentzian. This makes impossible a direct estimation of the single particle fermion width from the comparison of the meson production rate for different meson masses.

In Fig. 19 is also shown the semiclassical meson production rate calculated from the Eq. (A1) at zero meson momentum. For the equilibrium fermion momentum distribution we have taken the equilibrium momentum distribution at finite temperature :

$$f(p) = f_0\left(\frac{p^2}{2m}\right) \tag{B4}$$

or the momentum distribution including the quantum effect

$$f(p) = -i\int \frac{d\omega}{2\pi} G^<(p,\omega)\ . \tag{B5}$$

In the second case the rate of the meson production is much larger, reflecting the large momentum tail in the momentum distribution calculated from Eq. (B5). Similar large momentum tail is present in nuclear matter at zero temperature. This effect was found to be important for the semiclassical meson production in our nuclear collision model (Sect. II C). In Fig. 19 are shown also the semiclassical meson production rates for the width parameter $\gamma \to 0$. This strongly modifies the meson production rate for small meson mass. The meson production rate has a singularity for $m_s \to 0$. However, the nonzero γ parameter changes this behavior. The meson production rate stays finite for $m_s \to 0$ if $\gamma > 0$. This is similar to the Landau-Pomeranchuk-Migdal effect discussed in [2]. The semiclassical production cross section in medium is modified and has no singularity, even-though the meson production is given by the semiclassical expression (A1).

The quantum meson production rate is much larger than the semiclassical production rate in Fig. 9. However, such a comparison is not very meaningful. The Green's functions $G^{<(>)}$ used in the one-loop meson self energy (B1), where not calculated selfconsistently for a system of fermions interacting with potential V. On the other hand the interaction potential V enters in the expression for the semiclassical production rate of mesons.

REFERENCES

[1] W. Cassing, V. Metag, U. Mosel and K. Niita, Phys. Rep. **188**, 363 (1990).

[2] J. Knoll and N. Voskresenskii, Phys. Lett. **B351**, 43 (1995); Ann. Phys. **249**, 532 (1996).

[3] L.P. Kadanoff and G. Baym, Quantum Statistical Mechanics (Benjamin, New York, 1962).

[4] P. Danielewicz, Ann. Phys. **152**, 239 (1984).

[5] W. Botermans and R. Malfliet, Phys. Rep. **198**, 115 (1990).

[6] P. Danielewicz, Ann. Phys. **152**, 305 (1984).

[7] R. Malfliet, Nucl. Phys. **A545**, 3c (1992).

[8] H.S. Köhler, Phys. Rev. **C51**, 3232 (1995); Phys. Rev. **E53**, 3145 (1996).

[9] P.A. Henning, M. Blasone, R. Fauser and P. Zhuang, GSI-Preprint, GSI-96-57 (1996).

[10] A.G. Hall, J. Phys. **A8**, 214 (1975).

[11] T. Fujita and J. Hüfner, Nucl. Phys. **A314**, 317 (1979); T. Fujita, Nucl. Phys. **A324**, 409 (1979).

[12] The correlated initial state is not the stationary state of the BUU evolution equation. Thus, its use as the initial state is not consistent with the time dependent part of the evolution governed the BUU collision integral. However, it is motivated by the known quantum effects in the ground state fermion momentum distribution in nuclei.

[13] E. Oset, H. Toki and W. Weise, Phys. Rep. **83**, 281 (1982).

[14] P.V. Landshoff, Phys. Lett. **B386**, 291 (1996).

[15] P. Danielewicz, Ann. Phys. **197**, 154 (1990).

[16] P.A. Henning, Phys. Rep. **253**, 235 (1995).

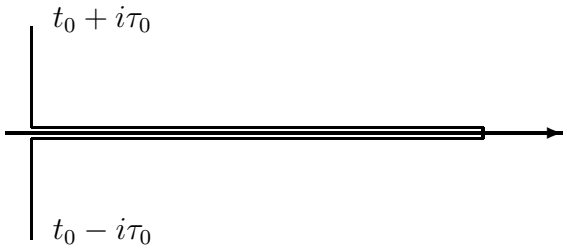

FIG. 1. The contour in the complex time plane on which the Green's functions are defined.

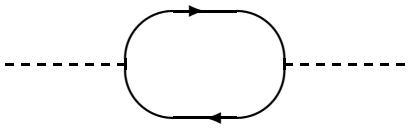

FIG. 2. The one-loop meson self-energy diagram. The solid lines are the fermion propagators, the dashed lines indicate the location of the meson-nucleon vertices.

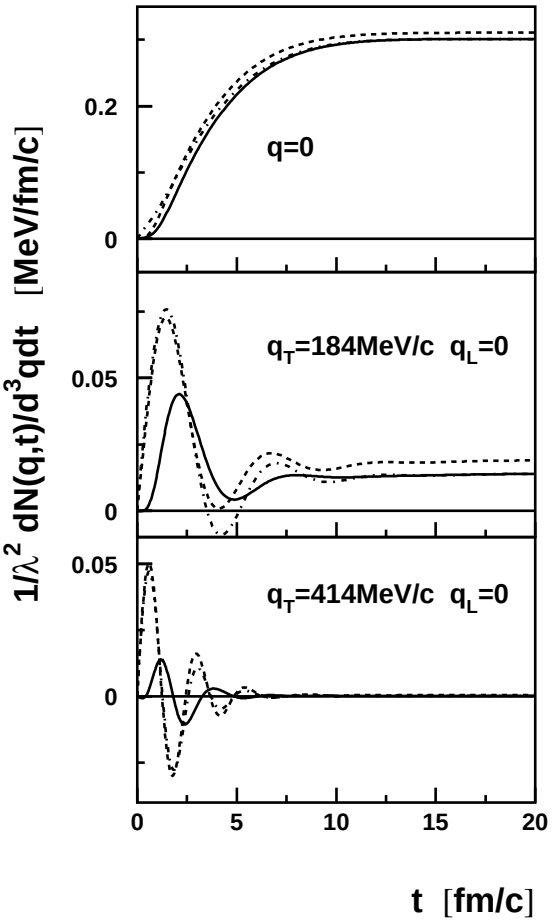

FIG. 3. Quantum rate of the production of mesons of mass $20MeV$ as a function of time. The dashed line is the meson production rate for the the uncorrelated initial state. The solid line is the meson production rate for the correlated initial state with both real and imaginary time integration in the meson production rate (12). The dashed-dotted line is the meson production rate for the correlated initial state with only real time integration in the meson production rate (12). The upper, middle and lower panel correspond to the transverse momentum of the produced meson of 0, 184 and $414MeV/c$ respectively. The energy of the collision is $180MeV$/nucleon.

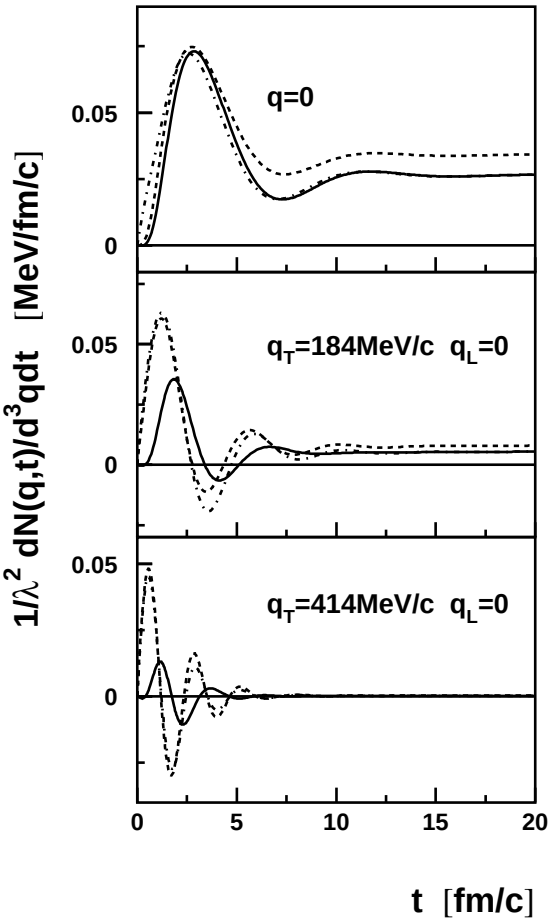

FIG. 4. Quantum rate of the production of mesons of mass $140MeV$ as a function of time. Details are similar as in Fig. 3

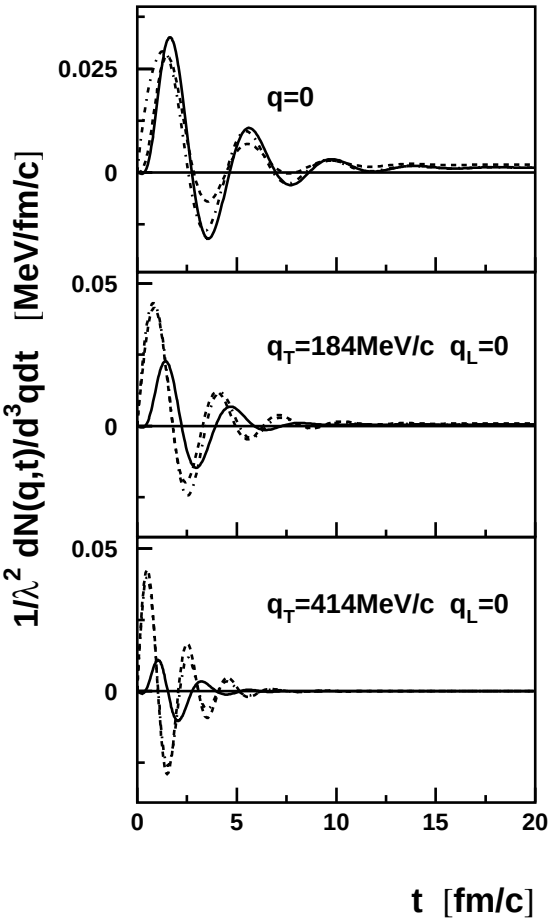

FIG. 5. Quantum rate of the production of mesons of mass $300MeV$ as a function of time. Details are similar as in Fig. 3

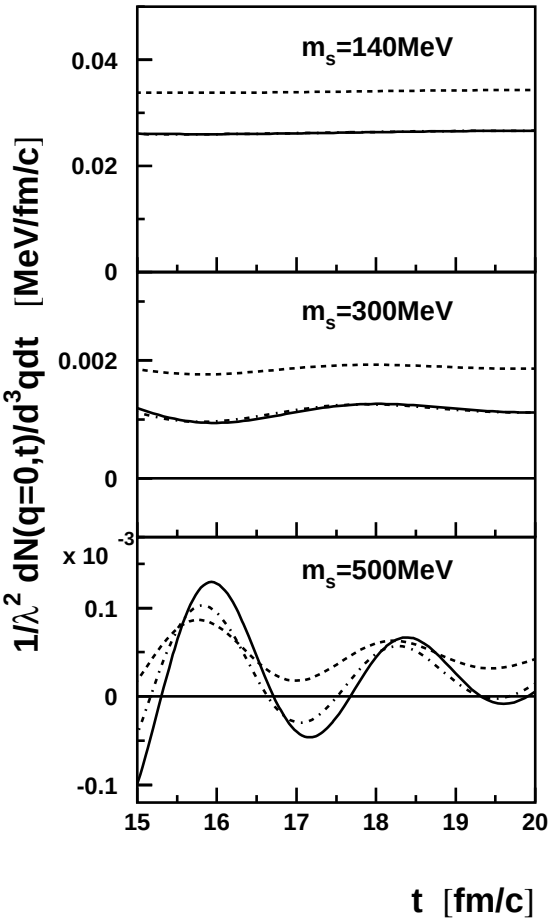

FIG. 6. Quantum rate of the production of mesons at zero momentum as a function of time. The dashed line is the meson production rate for the the uncorrelated initial state. The solid line is the meson production rate for the correlated initial state with both real and imaginary time integration in the meson production rate (12). The dashed-dotted line is the meson production rate for the correlated initial state with only real time integration in the meson production rate (12). The upper, middle and lower panel correspond to the mass of the produced meson of 140, 300 and $500MeV$ respectively. The energy of the collision is $180MeV$/nucleon.

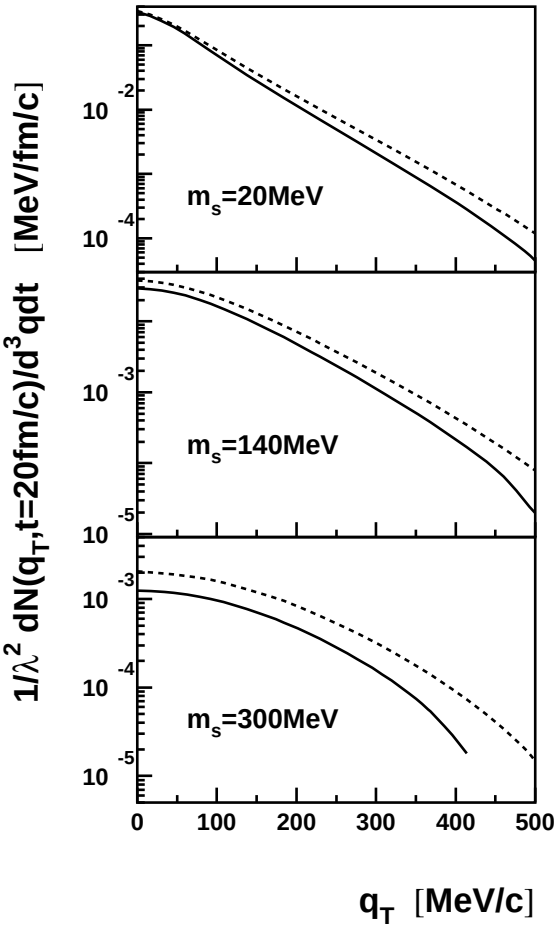

FIG. 7. Quantum rate of the production of mesons as a function of the transverse momentum at the end of the evolution ($t = 20fm/c$). The dashed line is the meson production rate for the uncorrelated initial state. The solid line is the meson production rate for the correlated initial state. The upper, middle and lower panel correspond to the mass of the produced meson of 20, 140 and $300MeV$ respectively. The energy of the collision is $180MeV$/nucleon.

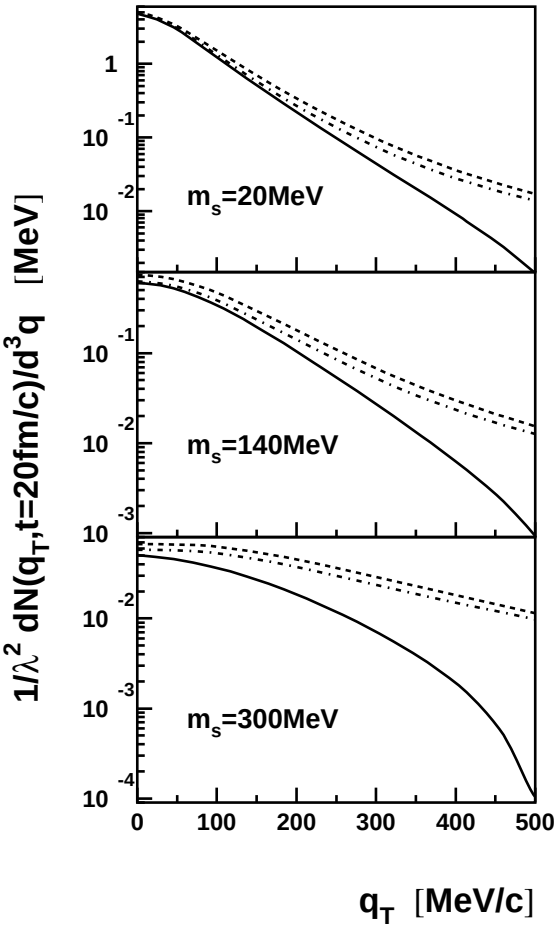

FIG. 8. The number of produced mesons as a function of the transverse momentum at the end of the evolution ($t = 20fm/c$) for the quantum one-loop meson production rate. The dashed line is the number of produced mesons for the the uncorrelated initial state. The solid line is the number of produced mesons for the correlated initial state with both real and imaginary time integration in the meson production rate (12). The dashed-dotted line is the number of produced mesons for the correlated initial state with only the real time integration in the meson production rate (12). The upper, middle and lower panel correspond to the mass of the produced meson of 20, 140 and $300MeV$ respectively. The energy of the collision is $180MeV$/nucleon.

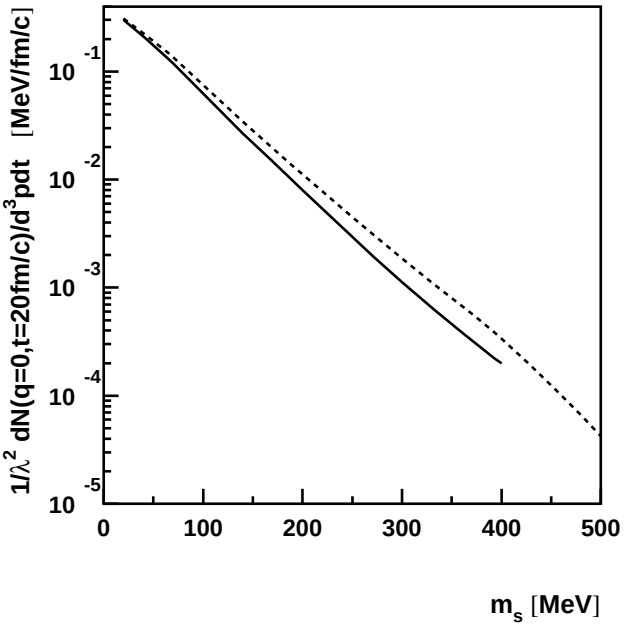

FIG. 9. Quantum rate of the production of mesons as a function of the meson mass at the end of the evolution ($t = 20fm/c$), for mesons with zero momentum. The dashed line is the meson production rate for the uncorrelated initial state. The solid line is the meson production rate for the correlated initial state. The energy of the collision is $180MeV$/nucleon.

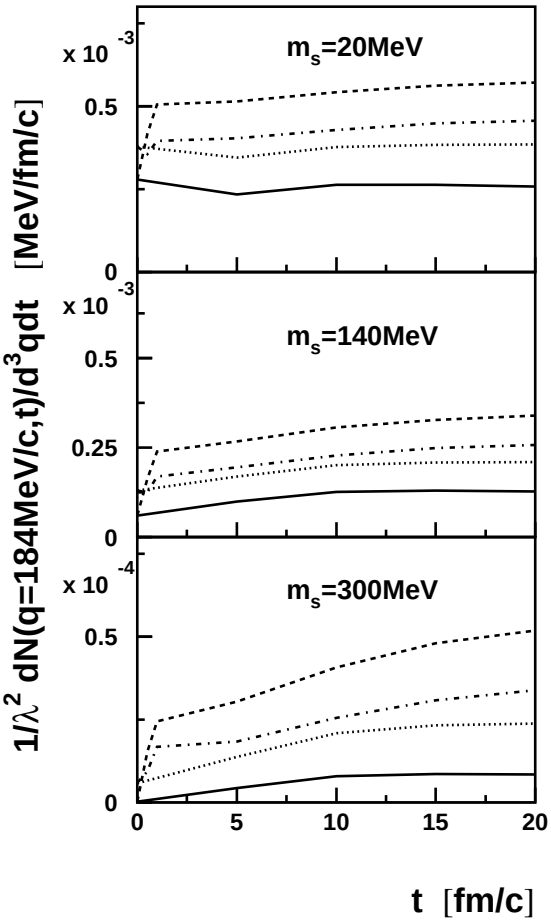

FIG. 10. Semiclassical rate of the production of mesons at momentum $q = 184MeV/c$ as a function of time. The solid and the dotted lines represent the semiclassical meson production rate for the BUU-like evolution of the fermion distribution from a Hartree and a correlated initial state respectively. The dashed and the dashed-dotted lines represent the semiclassical meson production rate for the quantum transport equations evolution of the fermion distribution from a Hartree and a correlated initial state respectively. The upper, middle and lower panel correspond to the mass of the produced meson of 140, 300 and $300MeV$ respectively. The energy of the collision is $180MeV$/nucleon.

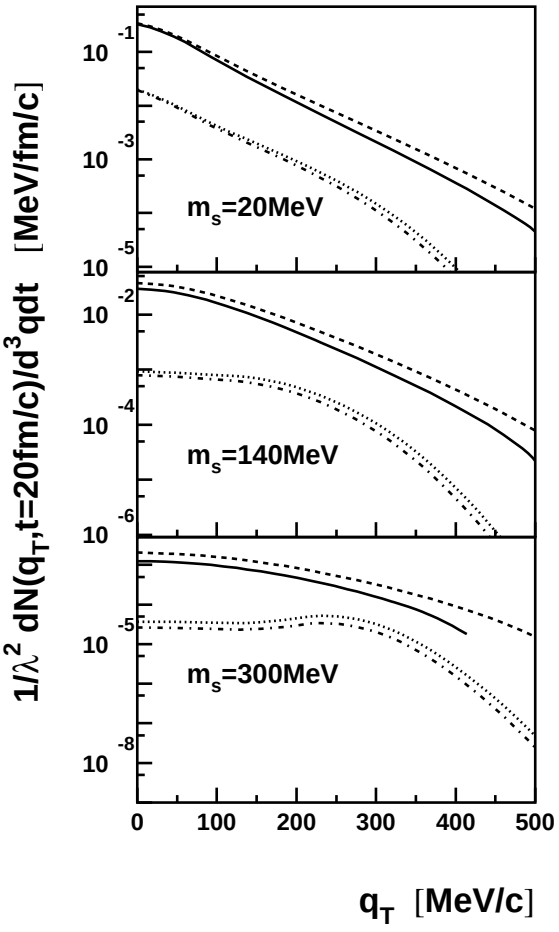

FIG. 11. Rate of the production of mesons as a function of the transverse momentum at the end of the evolution ($t = 20fm/c$). The dashed line is the quantum meson production rate for the uncorrelated initial state, the dotted line is the semiclassical meson production rate for the same final fermion momentum distribution. The solid line is the quantum meson production rate for the correlated initial state, the dashed-dotted line is the semiclassical meson production rate for the same final fermion momentum distribution. The upper, middle and lower panel correspond to the mass of the produced meson of 20, 140 and $300MeV$ respectively. The energy of the collision is $180MeV$/nucleon.

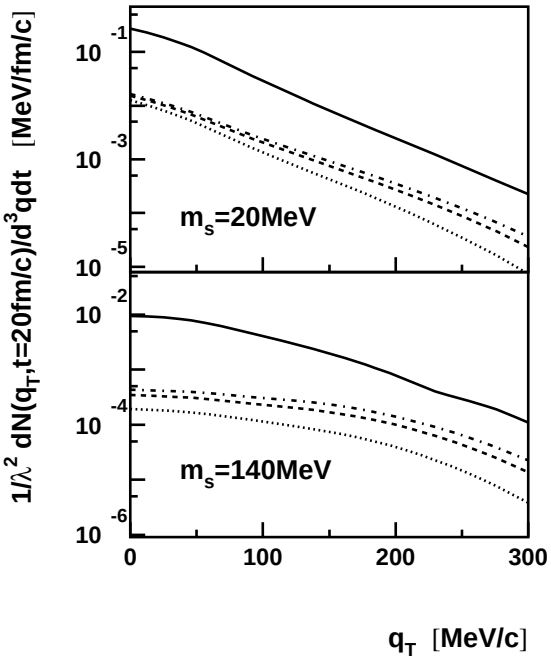

FIG. 12. Rate of the production of mesons as a function of the transverse momentum at the end of the evolution ($t = 20fm/c$). The solid line is the quantum meson production rate for the correlated initial state, the dashed-dotted line is the semiclassical meson production rate for the same final fermion momentum distribution. The dashed line is the semiclassical meson production rate for the BUU evolved correlated initial state. The dotted line is the semiclassical meson production rate for the BUU evolved Hartree initial state. The upper and lower panel correspond to the mass of the produced meson of 20 and $140MeV$ respectively. The energy of the collision is $110MeV$/nucleon.

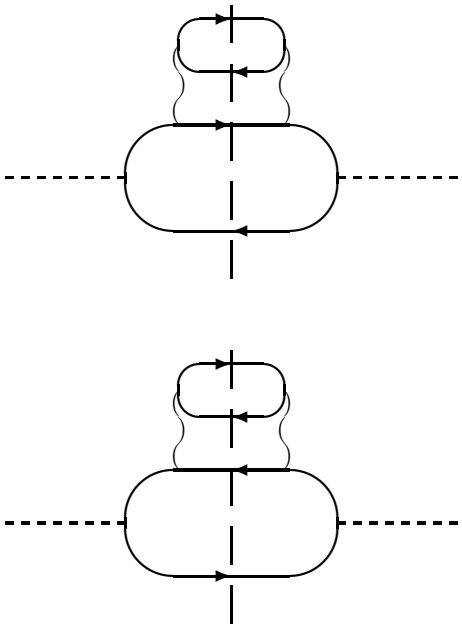

FIG. 13. The cut diagrams for the meson self-energy consisting of self-energy insertions on the fermion lines in the one-loop diagram. The wiggly line denotes the time local interaction, the cut is indicated by the long dashed line, other symbols as in Fig. 2.

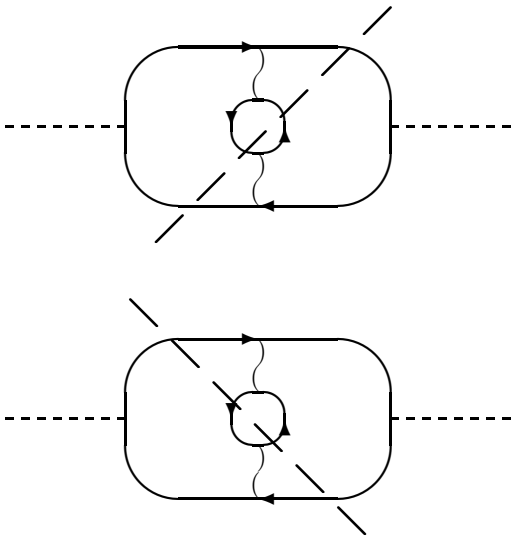

FIG. 14. The cut diagrams for the meson self-energy which are not self-energy insertions on the fermion lines in the one-loop diagram. Symbols as in Figs. 2 and 13.

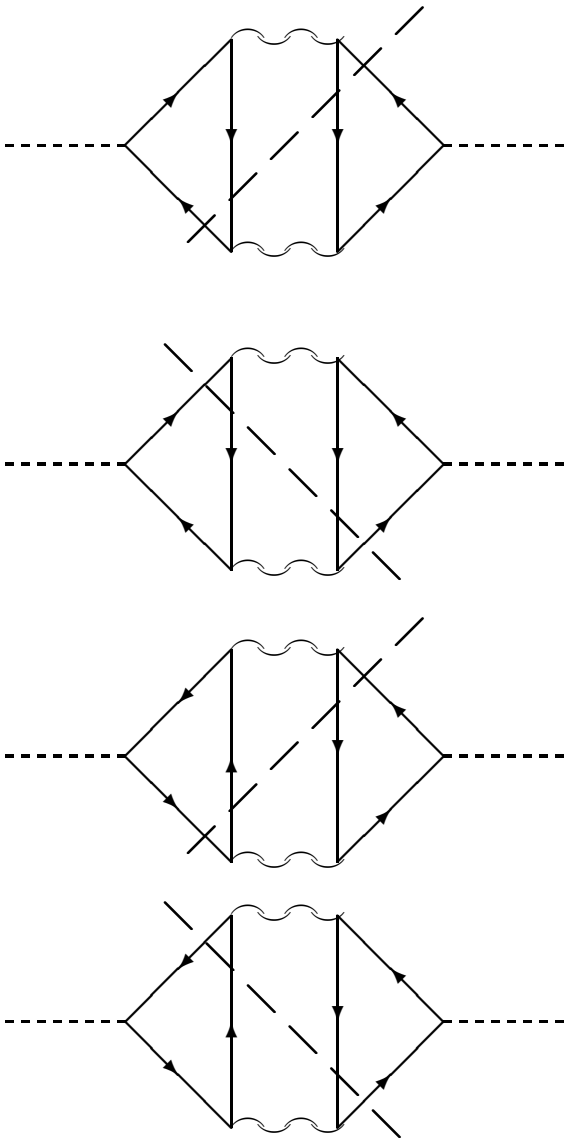

FIG. 15. The cut diagrams for the meson self-energy which are not self-energy insertions on the fermion lines in the one-loop diagram. These diagrams are zero for the pion-nucleon interaction vertex. Symbols as in Figs. 2 and 13.

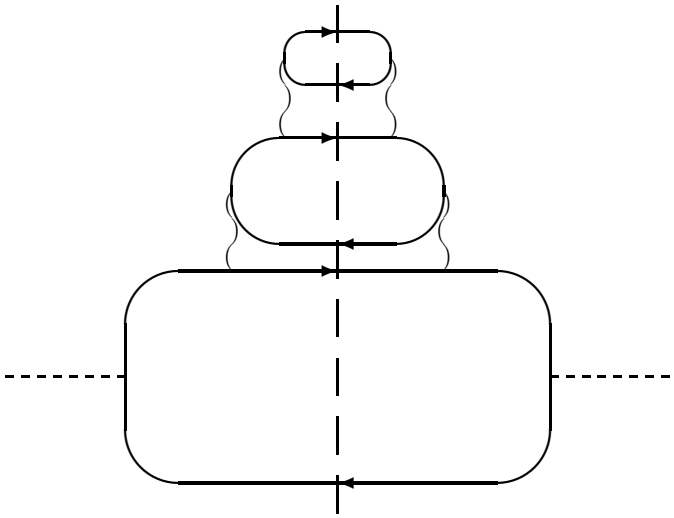

FIG. 16. A cut diagram for the meson self-energy of a type of direct Born self energy insertions on fermion lines. Many other self energy insertion can be added, giving after cutting processes involving many on-shell fermions. Symbols as in Figs. 2 and 13.

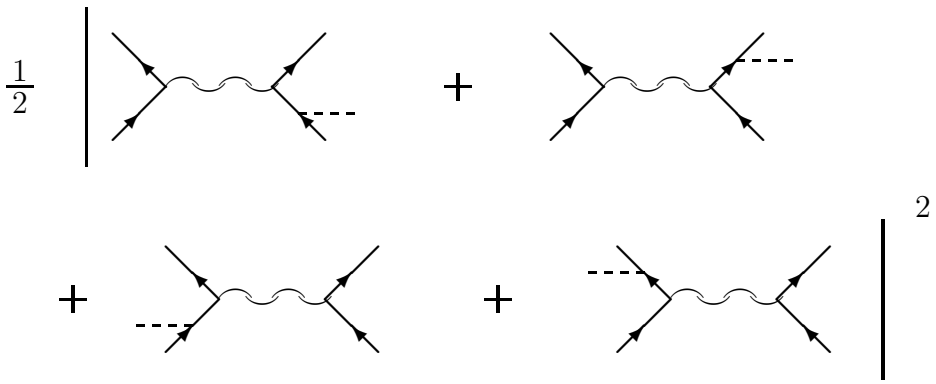

FIG. 17. The matrix element from the cut second order direct diagrams. See text for details.

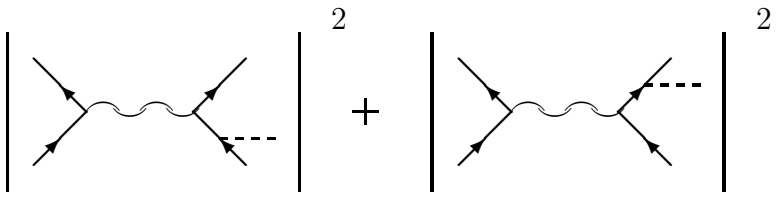

FIG. 18. The matrix element from the cut fermion self-energy insertion diagrams from Fig 13. See text for details.

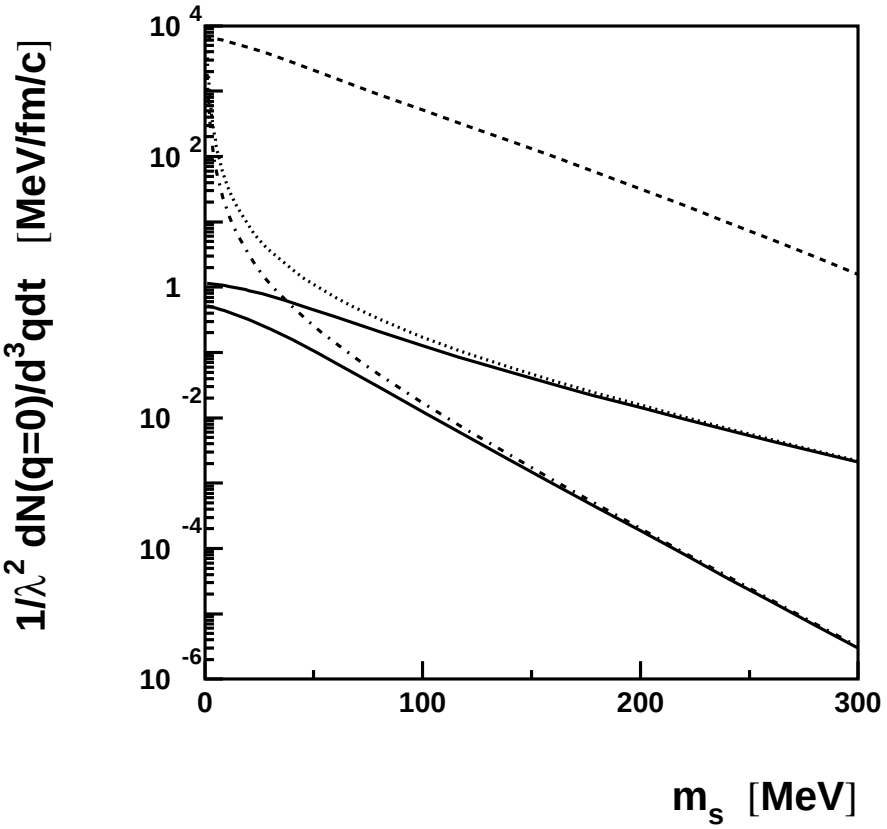

FIG. 19. Rate of meson production at zero momentum as a function of the meson mass. The dashed line is the quantum one-loop result (B3). The dotted line is the semiclassical production rate with the quantum equilibrium fermion momentum distribution and the dashed-dotted line is the the semiclassical production rate with the semiclassical equilibrium fermion momentum distribution ($\gamma \to 0$). The solid line close to the dotted line is the same as the dotted line but with a non-zero width ($\gamma = 60MeV$) of the retarded propagator in the calculation of the semiclassical production cross section. The solid line close to the dashed-dotted line is the same as the dashed-dotted line but with a non-zero width ($\gamma = 60MeV$) of the retarded propagator in the calculation of the semiclassical production cross section. The Fermi energy, the temperature and the width are 40, 30 and $60MeV$ respectively.